



Mitochondrial Network Size Scaling in Budding Yeast

Susanne M. Rafelski *et al.*

Science **338**, 822 (2012);

DOI: 10.1126/science.1225720

This copy is for your personal, non-commercial use only.

If you wish to distribute this article to others, you can order high-quality copies for your colleagues, clients, or customers by [clicking here](#).

Permission to republish or repurpose articles or portions of articles can be obtained by following the guidelines [here](#).

The following resources related to this article are available online at www.sciencemag.org (this information is current as of November 12, 2012):

Updated information and services, including high-resolution figures, can be found in the online version of this article at:

<http://www.sciencemag.org/content/338/6108/822.full.html>

Supporting Online Material can be found at:

<http://www.sciencemag.org/content/suppl/2012/11/08/338.6108.822.DC1.html>

This article **cites 31 articles**, 13 of which can be accessed free:

<http://www.sciencemag.org/content/338/6108/822.full.html#ref-list-1>

6. L. K. Nutt *et al.*, *Dev. Cell* **16**, 856 (2009).
 7. L. K. Nutt *et al.*, *Cell* **123**, 89 (2005).
 8. C. Bonzon, L. Bouchier-Hayes, L. J. Pagliari, D. R. Green, D. D. Newmeyer, *Mol. Biol. Cell* **17**, 2150 (2006).
 9. M. C. Wei *et al.*, *Science* **292**, 727 (2001).
 10. Materials and methods are available as supplementary materials on Science Online.
 11. W. Tirasophon, A. A. Welihinda, R. J. Kaufman, *Genes Dev.* **12**, 1812 (1998).
 12. X.-Z. Wang *et al.*, *EMBO J.* **17**, 5708 (1998).
 13. D. Han *et al.*, *Cell* **138**, 562 (2009).
 14. F. R. Papa, C. Zhang, K. Shokat, P. Walter, *Science* **302**, 1533 (2003).
 15. J. Krützfeldt *et al.*, *Nature* **438**, 685 (2005).
 16. A. Vermeulen *et al.*, *RNA* **13**, 723 (2007).
 17. D. P. Bartel, *Cell* **136**, 215 (2009).
 18. S. Yekta, I. H. Shih, D. P. Bartel, *Science* **304**, 594 (2004).
 19. H. I. Suzuki *et al.*, *Mol. Cell* **44**, 424 (2011).
 20. M. I. Almeida, R. M. Reis, G. A. Calin, *Mutat. Res.* **717**, 1 (2011).
 21. D. Long *et al.*, *Nat. Struct. Mol. Biol.* **14**, 287 (2007).
 22. A. K. Leung, P. A. Sharp, *Mol. Cell* **40**, 205 (2010).
 23. H. Puthalakath *et al.*, *Cell* **129**, 1337 (2007).
 24. D. Kieran, I. Woods, A. Villunger, A. Strasser, J. H. Prehn, *Proc. Natl. Acad. Sci. U.S.A.* **104**, 20606 (2007).
 25. A. G. Lerner *et al.*, *Cell Metab.* **16**, 250 (2012).

Acknowledgments: We thank R. Kaufman for *Atf6a*^{-/-} MEFs and D. Ron for *Perk*^{-/-} and *Ire1a*^{-/-} MEFs. The work was supported by NIH: DP2OD001925 (F.R.P.), R01CA136577 (S.A.O.), R01CA136717 (A.G.), R01DK080955 (F.R.P.), R01CA154916 (D.R.), GM080783 (M.T.M.), DK063720 (M.T.M.), and R01CA140456 (D.R.); Leukemia & Lymphoma Society Scholar Award (D.R.); Howard Hughes Medical Institute Physician-Scientist Early Career Award (S.A.O.); American Cancer Society Research Scholar Award (S.A.O.); Burroughs Wellcome Foundation (F.R.P.);

Hillblom Foundation (F.R.P.); Juvenile Diabetes Research Foundation (F.R.P.); Partnership for Cures (F.R.P.); National Science Foundation (E.S.W.); Susan G. Komen Foundation (A.G.); and an A*STAR Fellowship (L.L.). J.-P.U., L.W., D.H., E.S.W., N.H., and M.T. designed and performed experiments and contributed to the manuscript. L.L., M.T.M., D.R., and A.G. contributed key ideas, reagents, and data interpretation. F.R.P. and S.A.O. designed the study and wrote the manuscript. There are no conflicts of interest.

Supplementary Materials
www.sciencemag.org/cgi/content/full/science.1226191/DC1
 Materials and Methods
 Figs. S1 to S15
 Reference (26)

18 June 2012; accepted 10 September 2012
 Published online 4 October 2012;
 10.1126/science.1226191

Mitochondrial Network Size Scaling in Budding Yeast

Susanne M. Rafelski,^{1,2*†} Matheus P. Viana,^{3†} Yi Zhang,^{1,4} Yee-Hung M. Chan,^{1,2} Kurt S. Thorn,¹ Phoebe Yam,⁵ Jennifer C. Fung,⁵ Hao Li,^{1,2} Luciano da F. Costa,³ Wallace F. Marshall^{1,2,*}

Mitochondria must grow with the growing cell to ensure proper cellular physiology and inheritance upon division. We measured the physical size of mitochondrial networks in budding yeast and found that mitochondrial network size increased with increasing cell size and that this scaling relation occurred primarily in the bud. The mitochondria-to-cell size ratio continually decreased in aging mothers over successive generations. However, regardless of the mother's age or mitochondrial content, all buds attained the same average ratio. Thus, yeast populations achieve a stable scaling relation between mitochondrial content and cell size despite asymmetry in inheritance.

The amount of mitochondria in the cell varies in response to metabolic demands (1), requiring active size regulation mechanisms. The mitochondrial to cell size ratio is relatively constant in mammalian cells (2) and two yeast species (3, 4). We used the budding yeast *Saccharomyces cerevisiae* to study how the relationship between mitochondrial and cell size is achieved in cells growing and dividing asymmetrically (fig. S1). Yeast mitochondria

are three-dimensional (3D) networks of dynamic membrane-bound tubules localized at the cell periphery (5). To study mitochondrial size scaling, we developed a method to quantify the 3D skeletons of mitochondrial networks (Fig. 1A and fig. S2) using spinning disk confocal z-stacks of live yeast cells expressing mitochondrial matrix-targeted green fluorescent protein (GFP). We converted network length to mitochondrial volume (μm^3), assuming a constant tubule diameter. Absolute

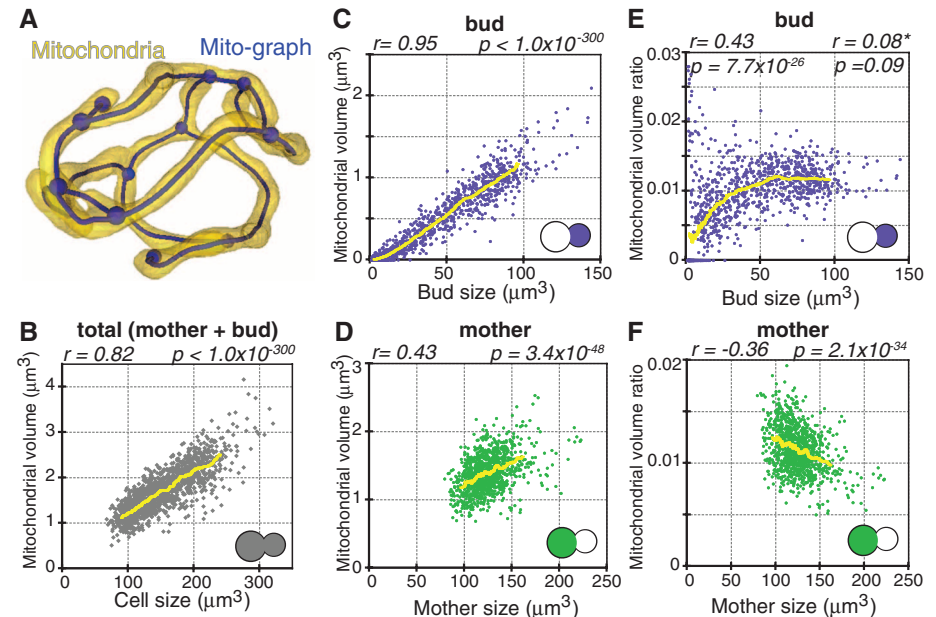
network length accuracy was within 85% of manual measurements, with an average reproducibility of 96% (6).

We imaged time courses of live yeast cells growing for one to two generations and measured the total cell and mitochondrial volumes for mother and bud compartments. We found a strong correlation between total mitochondrial and cell volumes (Fig. 1B). However, when we compared mother and bud compartments separately, the constant mitochondrial volume ratio found in the population as a whole was dominated by the scaling in the bud (Fig. 1, C and D). Mitochondrial volume ratio in the buds increased and then

¹Department of Biochemistry and Biophysics, University of California–San Francisco (UCSF), San Francisco, CA, USA. ²Center for Systems and Synthetic Biology, UCSF, San Francisco, CA, USA. ³Instituto de Física de São Carlos, Universidade de São Paulo, São Carlos, SP, Brazil. ⁴Center for Theoretical Biology and School of Physics, Peking University, Beijing, China. ⁵Department of Obstetrics, Gynecology, and Reproductive Sciences, UCSF, San Francisco, CA, USA.

*To whom correspondence should be addressed. E-mail: susanner@ucsf.edu (S.M.R.); wallace.marshall@ucsf.edu (W.F.M.)
 †Present address: Department of Developmental and Cell Biology, Center for Complex Biological Systems, University of California–Irvine, Irvine, CA, USA.

Fig. 1. Mitochondrial-cell size scaling is strongest in the bud. (A) Example of a mitochondrial network graph (blue), generated from 3D confocal images of a mitochondrion (yellow), imaged using matrix-targeted GFP in a live yeast cell. (B) Mitochondrial volume versus cell size for all cells analyzed in the time-course population ($n = 1430$ cells), including budding and nonbudding cells. The population maintained a consistent average mitochondrial to cell volume ratio. (C and D) Mitochondrial volume in the bud or mother and (E and F) Mitochondrial volume ratio in the bud or mother versus bud or mother size, respectively, for all budding cells ($n = 1053$ cells). (C and D) Buds displayed a much stronger correlation between mitochondrial and cell volume than mothers. Pearson's correlation coefficient, r , and significance value, P , are shown. Values for r and P on left and right sides in (E) are for the bud population greater/less than $40 \mu\text{m}^3$. Yellow lines indicate rolling average.



leveled off when buds were about half their final size (Fig. 1E). Bud size reflects the progression of budding, suggesting that buds accumulate mitochondria until they reach a set point of mitochondrial volume relative to bud size. In contrast, in mothers the mitochondrial volume ratio decreased with increasing cell size (Fig. 1F). Mother size reflects generational age (7), suggesting that older mothers do not preserve the mitochondrial volume ratio set point that they inherited when they were buds.

Analysis of the dynamics of cell growth and mitochondrial accumulation during budding time courses revealed dramatic asymmetry in mitochondrial accumulation between mother and bud (Fig. 2). During budding, mothers experienced an overall loss of both mitochondrial volume and the resultant volume ratio, while at the same time mitochondrial content increased in the bud proportional to bud growth (Fig. 2 and figs. S3 and S4). The mitochondrial accumulation rate in mothers was most negative at the moment that it was greatest in the bud (fig. S3B), suggesting that the bud might gain mitochondria at the expense of its mother. Although first and 2+ generation mothers differed significantly in cell size and mitochondrial content at the start of budding, the average kinetics of both bud growth

and mitochondrial accumulation in their buds was indistinguishable (Fig. 2C and fig. S3), resulting in the same average volume ratios at division (Fig. 2D). Thus, regardless of the initial size or mitochondrial content of mothers, they generate, on average, identical buds and do so with the same dynamics throughout budding.

Yeast cells displayed “mitochondrial content asymmetry” with a lower mitochondrial volume ratio in the mother than in the bud upon division (Fig. 2D). We asked whether mitochondrial content is replenished during the G1, unbudded, phase of the cell cycle. The mitochondrial volume ratio tended to increase for cells with lower, and decrease for cells with higher, initial volume ratios (Fig. 3A and fig. S5), suggesting a partial homeostatic restoration toward a unique mitochondrial volume ratio set point. We found no evidence that cells delayed G1 exit in response to a decreased volume ratio (fig. S6), but instead that cells may respond to deviations in the appropriate volume ratio by adjusting their rate of mitochondrial biogenesis (Fig. 3B and fig. S7). Analysis of mitochondrial content versus generational age (Fig. 3C) showed that sequential loss during budding and partial regain during G1 resulted in continual loss of mitochondrial volume ratio in aging mother

cells (Fig. 3D and figs. S8 and S9). However, these much older mothers still generated buds with the same average volume ratio at division. By generating buds with identical mitochondrial content, the population can renew and maintain a narrow distribution of mitochondrial volume ratios despite asymmetry in the inheritance of mitochondrial content between mother and bud (fig. S10).

There are two possibilities for how proper mitochondrial volume ratio is achieved in the bud: a passive mechanism not modulated as a function of mitochondrial content, where scaling would arise inherently [e.g., allometric growth (8)], or an active mechanism capable of sensing and feedback. In the passive case, a delay in mitochondrial inheritance would lead to fewer mitochondria entering the bud and a decreased volume ratio in the newborn mothers. In the active case, cells could sense and compensate for the delay to achieve the target volume ratio in the bud upon division. In *Δypt11* mutants, which exhibit delayed appearance of mitochondria in the bud (6, 9, 10), we found that while buds were delayed in mitochondrial inheritance (figs. S11 and S12), their volume ratio increased rapidly such that volume ratios in *Δypt11* and wild-type buds were indistinguishable at division (Fig. 4, A and B), consistent with an active mechanism. Meanwhile,

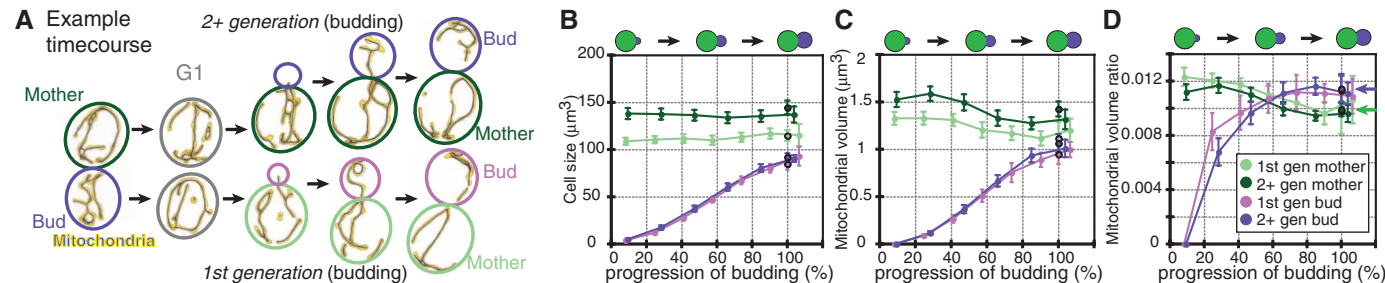


Fig. 2. Mitochondrial accumulation dynamics during progression of budding. (A) Overview of time-course experiment. First-generation mothers were considered separately from older, 2+, generation mothers. Yellow and blue represent mitochondria and network graphs. Colors for first generation (1st gen) and older generation (2+ gen) mothers and buds correspond to the colors used in all other figures. (B) Average cell size, (C) mitochondrial volume, and (D) mitochondrial volume ratio for mothers (green) and buds (purple) averaged throughout progression of budding, in percentage units where 100% is the average time until

division for that generation. Prediction data points, outlined in black, are included at time = 100%. Error bars: $\pm 95\%$ confidence intervals and numbers of cells in (6). (B) As expected, mothers grew very little (7), while the buds grew rapidly, with a peak growth rate halfway through budding (fig. S3A). (C) Mothers lost, while their buds gained, mitochondrial volume. (D) The resultant mitochondrial volume ratio in the bud increased and then plateaued (similar to Fig. 1E). At division, mothers had a significantly lower mitochondrial volume ratio than their buds. Arrows in (D) depict mean values; $P = 0.005$ by rank sum; $n = 25$ predivision cells.

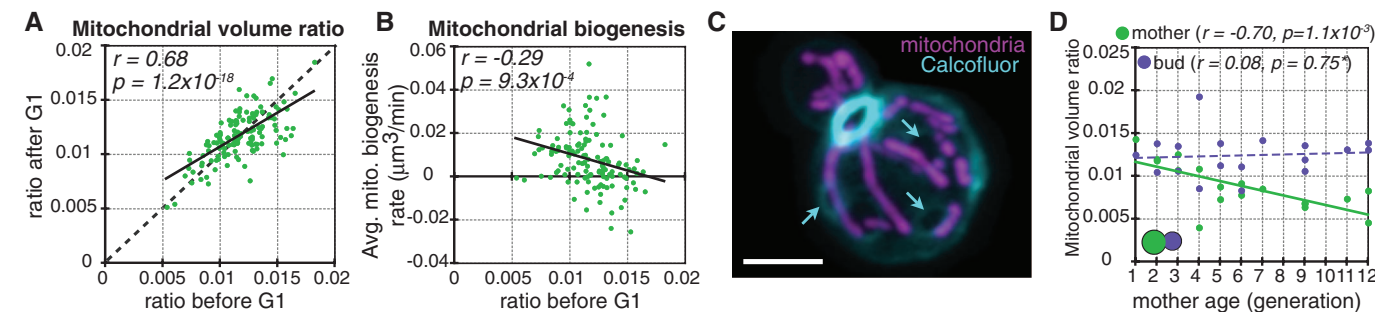
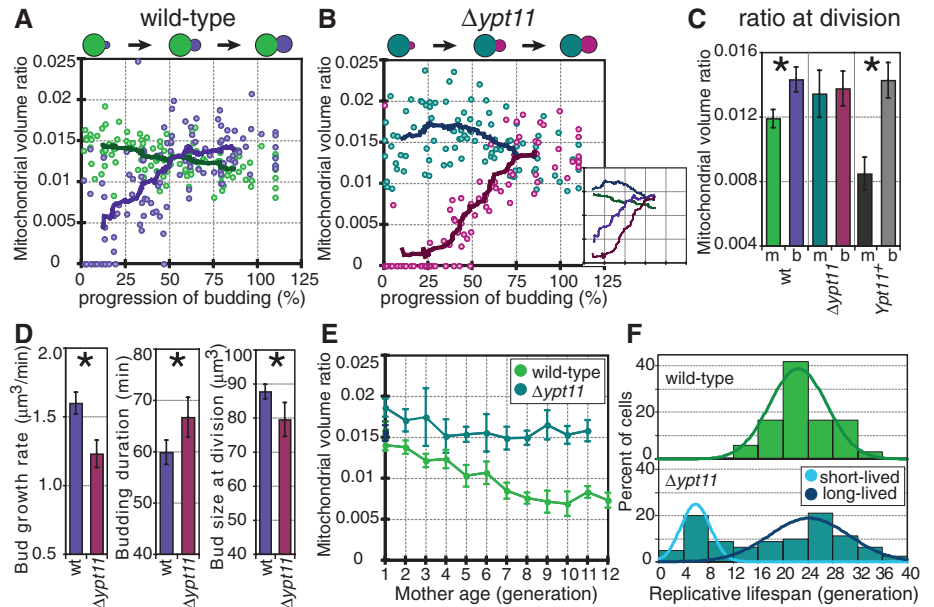


Fig. 3. Homeostatic control of mitochondrial content during cell aging. (A) In individual cells, mitochondrial volume ratio is strongly correlated between the start and end of G1 ($n = 130$ cells). Linear regression trendline (black) and line of equal volume ratio at the start and end of G1 (dotted) are shown. (B) Average mitochondrial biogenesis rate during G1 is negatively correlated with mitochondrial volume ratio at start of G1 ($n = 129$ cells). (C) Example of bud scar staining with Calcofluor (cyan) and mitochondria (magenta) for a mother

of generational age 10. Images are maximum intensity projections of a z-stack. Scale bar is $3\mu\text{m}$. Arrows point to three example bud scars. (D) Predivision mitochondrial volume ratio versus mother’s age for Calcofluor-labeled mothers (green) and buds (purple) (6). Volume ratio is maintained in buds but decreases in mothers as they age. Solid lines in (A), (B), and (D) represent statistically significant linear regression trendlines; Pearson’s correlation coefficient, r , and significance value, P , are shown. Dotted line in (D) represents the best-fit trendline.

Fig. 4. Mitochondrial accumulation dynamics and aging in $\Delta ypt11$ mutant. (A) Wild-type and (B) $\Delta ypt11$ buds reach the same mitochondrial volume ratio at division despite different accumulation dynamics during budding. Mitochondrial volume ratio of (A) wild-type and (B) $\Delta ypt11$ mothers (green and turquoise, respectively) and buds (purple and magenta, respectively) as a function of progression of budding. Average time-course behavior was obtained by converting bud sizes from single time-point data into progression of budding (fig. S16). Thick and thin lines indicate the rolling average and 95% confidence interval, respectively. (C) Ypt11p is involved in generating mother-daughter mitochondrial content asymmetry. The average mitochondrial volume ratio at division for wild-type ($n = 39$ cells), $\Delta ypt11$ ($n = 28$ cells), and Ypt11p-overexpressing (Ypt11+) ($n = 36$ cells) (12) mothers (m) and buds (b). Asterisks: $P = 1.9 \times 10^{-5}$ and 5.6×10^{-9} by rank sum. (D) Average bud growth rate, duration of budding ($n = 56$ and 24 cells for wild-type and $\Delta ypt11$ buds, respectively), and bud size at division ($n = 106$ and 53 cells, respectively) for wild-type (purple) and $\Delta ypt11$ (magenta) buds during budding. Asterisks: $P = 5.3 \times 10^{-6}$, $<1 \times 10^{-14}$, and 4.6×10^{-4} by rank sum. (E) Age-dependent loss of mitochondrial volume ratio from mothers. The average mitochondrial volume ratio for wild-type (green) and $\Delta ypt11$ (turquoise) mothers of increasing generational age. Darker first-generation data points represent average values of mothers at their “birth” (6). Error bars: $\pm 95\%$ confidence intervals and numbers of cells in (6). (F) Replicative life-span histogram for wild-type (green, $n = 36$



mother mitochondrial content increased transiently, presumably because mitochondria could not be redistributed into the buds. Mother-daughter mitochondrial content asymmetry was thus eliminated in the absence, and was enhanced with overexpression, of Ypt11p (Fig. 4C), suggesting that Ypt11p contributes to this asymmetry. However, in all three cases, the proper volume ratio was achieved in the bud at division. We thus propose that yeast cells can somehow sense mitochondrial accumulation kinetics in the bud and respond to ensure that the target volume ratio is achieved in time for division. The compensatory behavior observed in $\Delta ypt11$ mutants likely involves one or both of the remaining mitochondrial inheritance pathways (6, 10), which themselves may also contribute to mother-daughter mitochondrial content asymmetry.

$\Delta ypt11$ buds could potentially reach the proper mitochondrial volume ratio by slowing their growth and “waiting” for the delayed mitochondrial content to catch up. We analyzed time courses of $\Delta ypt11$ cells and found that buds indeed grew at slower rates and for a longer time before division (Fig. 4D). Mutants with the longest budding durations exhibited greatly decreased mitochondrial volume ratios at the time when normal $\Delta ypt11$ cells would divide (fig. S13). However, $\Delta ypt11$ cells divided with buds of a smaller size than wild-type buds, suggesting, unexpectedly, that cell size may be affected by mitochondrial inheritance kinetics. Yeast cell size is known to respond to changes in metabolism brought about by nutritional environment (11), suggesting perhaps that a delay in mitochondrial inheritance somehow altered the cell’s metabolic state even though its environment remained unchanged.

We tested whether simply delaying redistribution of mitochondria into the bud could alter the age-dependent loss of volume ratio observed in wild-type mothers (Fig. 3D). Aging $\Delta ypt11$ mothers lost mitochondrial volume ratio much more slowly than wild-type mothers (Fig. 4E and fig. S14). Replicative life-span distributions of $\Delta ypt11$ mutants (6) were similar to $\Delta mnr1$ mitochondrial inheritance mutants (12). The $\Delta ypt11$ distribution was statistically bimodal (6), consisting of a shorter-lived population, not seen in wild type, and a longer-lived population with both a slightly increased average and significantly increased maximum life span compared with wild type (Fig. 4F and fig. S15) (6). Because of their decreased life spans, short-lived $\Delta ypt11$ cells represent a decreasing proportion of the aging $\Delta ypt11$ population (e.g., 19 and 5% of cells at generations 6 and 10). Thus, the $\Delta ypt11$ cells with increased mitochondrial volume ratios at later generations consisted almost entirely of the second population with a longer life span than wild-type cells. Thus, in addition to the quality of mitochondria retained in the mother (12), their quantity may also contribute to their replicative life spans.

The failure of mother cells to maintain mitochondrial volume ratio suggests that they either cannot sense reduced content or are unable to compensate for the loss. Failing to preserve her own mitochondrial volume ratio could be the cost incurred for generating the healthiest, fittest offspring upon division.

References and Notes

1. A. Devin, M. Rigoulet, *Toxicol. Mech. Methods* **14**, 271 (2004).
2. J. W. Posakony, J. M. England, G. Attardi, *J. Cell Biol.* **74**, 468 (1977).

3. K. Tanaka, T. Kanbe, T. Kuroiwa, *J. Cell Sci.* **73**, 207 (1985).
4. M. Uchida *et al.*, *Yeast* **28**, 227 (2011).
5. J. Nunnari *et al.*, *Mol. Biol. Cell* **8**, 1233 (1997).
6. Materials and methods are available as supplementary materials on Science Online.
7. C. L. Woldring, P. G. Huls, N. O. Vischer, *J. Bacteriol.* **175**, 3174 (1993).
8. J. S. Huxley, G. Teissier, *Nature* **137**, 780 (1936).
9. T. Itoh, A. Watabe, A. Toh-E, Y. Matsui, *Mol. Cell. Biol.* **22**, 7744 (2002).
10. R. L. Frederick, K. Okamoto, J. M. Shaw, *Genetics* **178**, 825 (2008).
11. J. J. Turner, J. C. Ewald, J. M. Skotheim, *Curr. Biol.* **22**, R350 (2012).
12. J. R. McFaline-Figueroa *et al.*, *Aging Cell* **10**, 885 (2011).

Acknowledgments: We thank J. Nunnari, J. Shaw, and A. Lewandowska for plasmids, strains, and discussions; G. Pesce for sharing unpublished results and discussions; and A. Caudy, E. Hong, K. C. Huang, A. Rosebrock, and the Marshall laboratory for reading the manuscript. Microscopy was performed at the UCSF Nikon Imaging Center. This work was supported by Sandler and Boyer Postdoctoral Fellowships (S.M.R.); the Herbert Boyer Junior Faculty Endowed Chair Award and NIH grant R01GM097017 (W.F.M.); an NIH National Research Service Award fellowship (Y.-H.M.C.); Fundação de Amparo à Pesquisa do Estado de São Paulo (05/00587-5, 07/50882-9) and Conselho Nacional de Desenvolvimento Científico e Tecnológico (301303/06-1) grants (L.d.F.C. and M.P.V.); NIH grants R01GM070808, R01GM026259, P50GM081879, and a Packard Fellowship (Y.Z. and H.L.); a China Scholarship Council (CSC) scholarship (Y.Z.); and NIH grant 5R01GM097213-02 (P.Y. and J.C.F.). Image analysis algorithms are described in detail in methods (6). The data are included in the main and supplementary figures.

Supplementary Materials

www.sciencemag.org/cgi/content/full/338/6108/822/DC1
 Materials and Methods
 Figs. S1 to S21
 References (13–32)

6 June 2012; accepted 18 September 2012
 10.1126/science.1225720